Dalton Transactions

Accepted Manuscript

ROYAL SOCIETY OF CHEMISTRY

www.rsc.org/dalton

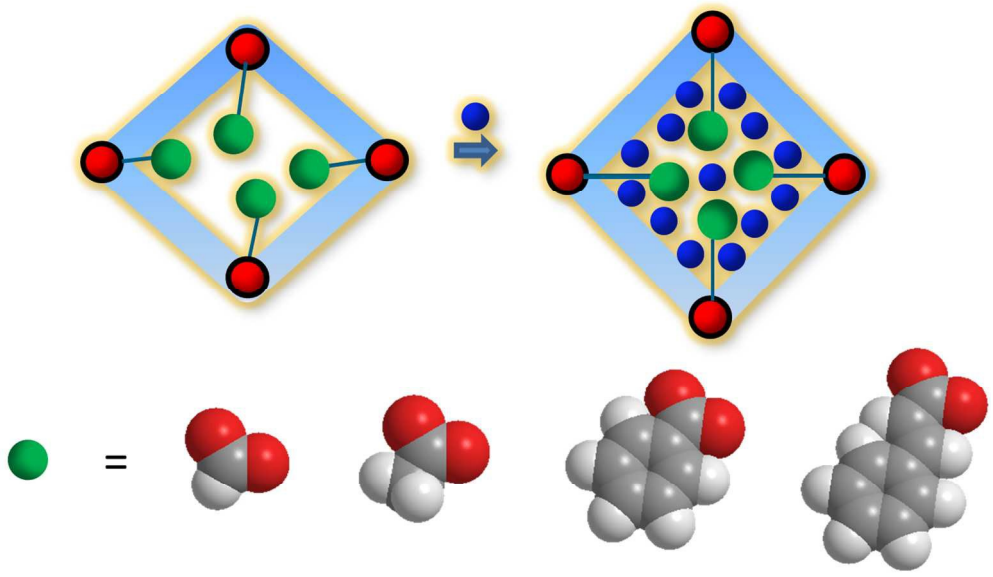

124x72mm (300 x 300 DPI)

Dalton transactions

ARTICLE

Tuning the flexibility in MOFs by SBU functionalization

Volodymyr Bon,[a] Negar Kavoosi,[a] Irena Senkovska,[a] Philipp Müller,[a] Jana Schaber,[b] Dirk Wallacher,[c] Daniel M. Többens,[d] Uwe Mueller,[e] and Stefan Kaskel[a*]

Received 00th January 20xx,
Accepted 00th January 20xx

DOI: 10.1039/x0xx00000x

www.rsc.org/

A new approach for the fine tuning of flexibility in MOFs, involving functionalization of the secondary building unit, is presented. The "gate pressure" MOF $[Zn_3(bpydc)_2(HCOO)_2]$ was used as a model material and SBU functionalization was performed by using monocarboxylic acids such as acetic, benzoic, or cinnamic acids instead of formic acid in the synthesis. The crystal structures of resulting materials are isomorphous to that of $[Zn_3(bpydc)_2(HCOO)_2]$ in the "as made" form, but show different structural dynamics during the guests removal. The activated materials have entirely different properties in the nitrogen physisorption experiments clearly showing the tunability of the gate pressure, at which the structural transformation occurs, by using monocarboxylic acids with varying backbone structure in the synthesis. Thus, increasing number of carbon atoms in the backobone leads to the decreasing gate pressure required to initiate the structural transition. Moreover, *in situ* adsorption/PXRD data suggests differences in the mechanism of the structural transformations: from "gate openning" in the case of the formic acid to "breathing" if benzoic acid is used.

Introduction

Flexible Metal-Organic Frameworks (MOFs) or so called Soft Porous Crystals are a unique class of materials capable to switch between the porous and dense (or less porous) states as a response to external stimuli such as temperature, pressure, electromagnetic irradiation or adsorption of guest molecules.[1-3] The existence of two different states with different physical and textural properties gives rise to a wide potential application field of such materials. For example, NH_2-MIL-53(Al) is able to transform between the narrow and large pore phase and therefore could be used as an optical switch.[4] Sensor technology is also one of the prospective applications fields for switchable MOFs. Thus the Mg based flexible MOF with the composition $[Mg(H_2dhtp)(H_2O)_2]\cdot DMAc$, denoted as AEMOF-1·DMAc (AEMOF-1 - alkaline earth MOF-1; H_4dhtp - 2,5-dihydroxy-terepthalic acid; DMAc - *N,N'*-dimethylacetamide) was used as a highly efficient luminescent sensor for the real time detection of water traces in various organic solvents.[5] The flexibility was also successfully used to achieve the separation of CO and N_2, which have very similar physical properties.[6] The selective trapping of NO molecules in the flexible Ru- and Rh-based coordination polymers could find its application in biomedicine.[7]

All envisioned applications based on the flexibility require materials with well-defined switching behavior. However, tuning and designing of flexible MOFs with specific switching properties remain very challenging, which limits the application potential of flexible crystalline materials. The most often applied strategies to influence the flexibility in a soft MOFs[8] are: i) introducing of flexible side chains into the ligand;[9] ii) modulation of host–guest interaction strength by linker functionalization;[10] iii) incorporation of different metals into the same framework;[11] iv) adjustment of the crystal size.[12]

In this contribution we present an switchability tuning approach based on the systematic substitution of monocarboxylates in the secondary building unit (SBU) of a "gate pressure" MOF $[Zn_3(bpydc)_2(HCOO)_2]$ (bpydc - 2,2'-bipyridyl-5,5'-dicarboxylate), also known as JLU-Liu4 (JLU - JiLin University).[13] It contains two formic acid anions directly coordinated to the metal cluster. The solvent assisted exchange of monocarboxylic ligand was already demonstrated for rigid Zr based MOFs.[14] We could show that utilizing monocarboxylic acids with different backbone in the synthesis (for instance acetic, benzoic, or cinnamic acid) results in the formation of isomorphous frameworks, showing completely different adsorption behavior. Crystal structures of the large pore and narrow pore phases as well as adsorption behavior of the materials bearing different monocarboxylic ligands were studied to enlighten the structural transformations in quest.

Experimental

[a] *Department of Inorganic Chemistry, Technische Universität Dresden, Bergstrasse 66, D-01062 Dresden, Germany*
[b] *Department of Bioanalytical Chemistry, Technische Universität Dresden, Bergstrasse 66, D-01062 Dresden, Germany*
[c] *Department of Sample Environments, Helmholtz-Zentrum Berlin für Materialien und Energie, Hahn-Meitner-Platz 1, 14109 Berlin, Germany*
[d] *Department of Crystallography, Helmholtz-Zentrum Berlin für Materialien und Energie, Hahn-Meitner-Platz 1, 14109 Berlin, Germany*
[e] *MX Group, Institute for Soft Matter and Functional Materials, Helmholtz-Zentrum Berlin für Materialien und Energie, Albert-Einstein-Str. 15, 12489 Berlin, Germany*
† Corresponding author: Prof. Stefan Kaskel, *E-mail: Stefan.Kaskel@tu-dresden.de*
Electronic Supplementary Information (ESI) available: Temperature dependent PXRD measurement for **1'**, TG curves for **2'-4'**, FT-IR spectra for **1'-4'**, PXRD patterns for **3'** and **4'**. See DOI: 10.1039/x0xx00000x

Materials

All chemicals were purchased from commercial sources and used without further purification. *N,N*-dimethylformamide (DMF) (anhydrous 99.8 %), trans-cinnamic acid (97 %), acetonitrile (99.8 %), and 5,5′-dimethyl-2,2′-dipyridyl (98 %, dmpby) were purchased from Sigma Aldrich. 2,2′-bipyridyl-5,5′-dicarboxylic acid (H_2bpydc) was synthesised according to the reported procedure[15] (for more details see ESI). Benzoic acid (99.5 %) and formic acid (99 %) were purchased from Grüssing GmbH, $Zn(NO_3)_2{\cdot}4H_2O$ from MERCK, acetic acid (100 %) from ROTH Company, heptane (99 %) and dichloromethane 9.99 % from Fisher, anhydrous toluene from VWR, and 1-propanol 99.5 % from TCI.

Synthesis

$[Zn_3(bpydc)_2(HCOO)_2]$ JLU-Liu4 (1)

JLU-Liu4 (**1**) was synthesized using slightly modified procedure. $Zn(NO_3)_2{\cdot}4H_2O$ (52.2 mg, 0.2 mmol), H_2bypdc (20 mg, 0.082 mmol) and formic acid (1 mL, 26.5 mmol) were mixed with 6.5 mL DMF and transferred to the Pyrex© tubes. The mixture was heated for 24 h at 120 °C. The resulting white octahedral crystals were filtered and washed 3 times with DMF. Filtration was performed under argon flow. After that, the solvent was exchanged to ethanol over a period of 3 days. At the end, the sample was activated for 5 hours at 70 °C using dynamic vacuum. Yield: 32.2 mg (63 %). After activation, all samples were handled under argon atmosphere. PXRD patterns measured for "as made" and activated samples confirmed the phase purity.

$[Zn_3(bpydc)_2(CH_3COO)_2]$ (2)

A mixture of $Zn(NO_3)_2{\cdot}4H_2O$ (52.2 mg, 0.2 mmol), H_2bypdc (20 mg, 0.082 mmol), and acetic acid (1 mL, 26.5 mmol) with 6.5 mL DMF was added to Pyrex© tubes and heated 24 h at 120 °C. Then crystals were collected and washed several times first with DMF and then with ethanol. Subsequently, they were immersed in dry ethanol for 3 days. The crystals were filtered in argon flow and evacuated for 12 h at 70 °C. Yield: 17.26 mg (52.5 %).

Elemental analysis (wt.%): calc. C 42.89, N 6.98, H 2.74; found C 41.13, N 7.26, H 1.03.

$[Zn_3(bpydc)_2(C_6H_5COO)_2]$ (3)

$Zn(NO_3)_2{\cdot}4H_2O$ (52.2 mg, 0.2 mmol), H_2bypdc (20 mg, 0.082 mmol), and benzoic acid (1.4 g, 11.5 mmol) were dissolved in 6.5 mL DMF. The mixture was placed into the Pyrex© tubes and heated at 120 °C for 48 h. Washing and activation procedures were the same as described for compound **2**. Yield: 16 mg (42.65 %).

Elemental analysis (wt.%): calc. C 49.23, N 6.04, H 2.8; found C 48.18, N 6.16, H 1.27.

$[Zn_3(bpydc)_2(C_6H_5CHCHCOO)_2]$ (4)

A mixture of $Zn(NO_3)_2{\cdot}4H_2O$ (52.2 mg, 0.2 mmol), H_2bypdc (20 mg, 0.082 mmol), and cinnamic acid (1.25 g, 8.4 mmol) with 6.5 mL DMF was placed into the Pyrex© tubes and heated at 80 °C for 72 h. Washing and activation procedures were the same as described for compound **2**. Yield: 21 mg (53 %).

Elemental analysis (wt.%): calc. C 51.52, N 5.72, H 3.06; found C 49.77, N 5.87, H 1.96.

Single crystal X-ray diffraction

The crystal structure of compounds **1** - **4** were determined by single crystal X-ray diffraction. All single crystals were prepared in glass capillaries with some amount of solvent. The capillaries were sealed with melted wax. The datasets were collected at BESSY MX BL14.2 beamline of Helmholtz-Zentrum Berlin für Materialien und Energie (HZB).[16] All diffraction experiments were performed at room temperature using the radiation with energy of 14 keV (λ = 0.88561 Å). The *φ*-scans with oscillation range of 1° were used for data collection. The datasets were processed using CCP4 software.[17] The crystal structures were solved by direct methods and refined by full matrix least-squares on F^2 using SHELXTL program package.[18] All non-hydrogen atoms were refined in anisotropic approximation. Hydrogen atoms were refined in geometrically calculated positions using "riding model" with $U_{iso}(H) = 1.2U_{iso}(C)$ for sp, sp^2 hybridized carbon atoms and with $U_{iso}(H) = 1.5U_{iso}(C)$ for sp^3 hybridized carbon atoms. The atoms of phenyl rings in benzoate (compound **3**) and cinnamate (compound **4**) anions are disordered and were treated using AFIX 66 instruction. In the case of compound **4**, SIMU and DELU instructions has been used to restrain the thermal parameters of disordered fragments. Because of the high symmetry of the crystal system it was not possible to localize the lattice solvent molecules in the pores. Therefore, the SQUEEZE procedure was used to correct reflection intensities, corresponding to disordered solvent molecules.[19] CCDC-1422814, CCDC-1422816, CCDC-1422818, and CCDC-1422820 contain the supplementary crystallographic data for compounds **1, 2, 3,** and **4,** correspondingly. These data can be obtained free of charge from the Cambridge Crystallographic Data Centre via www.ccdc.cam.ac.uk/data_request/cif. The extended crystallographic data for the structures **1** - **4** are given in Tables S1 of ESI.

Crystal data for $[Zn_3(bpydc)_2(HCOO)_2]$ (1): $C_{26}H_{14}N_4O_{12}Zn_3$, M = 770.52 g mol^{-1}, tetragonal, $P4_32_12$ (Nr. 96), a = 15.320(2) Å, c = 23.240(5) Å, V = 5454.5(18) $Å^3$, Z = 4, ρ_{calc}= 0.938 g cm^{-3}, λ = 0.88561 Å, T = 298 K, Θ_{max} = 32.1°, reflections collected/unique 12822/5847, R_{int} = 0.0194, R_1 = 0.0287, wR_2 = 0.0852, S = 1.089, largest diff. peak 0.569 e $Å^{-3}$ and hole -0.543 e $Å^{-3}$.

Crystal data for $[Zn_3(bpydc)_2(CH_3COO)_2]$ (2): $C_{28}H_{18}N_4O_{12}Zn_3$, M = 798.57 g mol^{-1}, tetragonal, $P4_32_12$ (Nr. 96), a = 15.300(2) Å, c = 23.280(5) Å, V = 5449.6(18) $Å^3$, Z = 4, ρ_{calc}= 0.973 g cm^{-3}, λ = 0.88561 Å, T = 298 K, Θ_{max} = 32.1°, reflections collected/unique 19800/6337, R_{int} = 0.0275, R_1 = 0.0313, wR_2 = 0.0960, S = 1.099, largest diff. peak 0.629 e $Å^{-3}$ and hole -0.532 e $Å^{-3}$.

Crystal data for $[Zn_3(bpydc)_2(C_6H_5COO)_2]$ (3): $C_{38}H_{22}N_4O_{12}Zn_3$, M = 922.70 g mol^{-1}, tetragonal, $P4_32_12$ (Nr. 96), a = 15.160(2) Å, c = 23.030(5) Å, V = 5292.9(18) $Å^3$, Z = 4, ρ_{calc}= 1.158 g cm^{-3}, λ = 0.88561 Å, T = 298 K, Θ_{max} = 32.1°, reflections collected/unique 40507/6196, R_{int} = 0.0556, R_1 = 0.0515, wR_2 = 0.1546, S = 1.079, largest diff. peak 0.656 e $Å^{-3}$ and hole -0.764 e $Å^{-3}$.

Crystal data for $[Zn_3(bpydc)_2(C_6H_5CH{=}CHCOO)_2]$ (4): $C_{42}H_{26}N_4O_{12}Zn_3$, M = 974.78 g mol^{-1}, tetragonal, $P4_32_12$ (Nr. 96), a = 15.270(2) Å, c = 23.050(5) Å, V = 5374.6(18) $Å^3$, Z = 4, ρ_{calc}= 1.205 g cm^{-3}, λ = 0.88561 Å, T = 298 K, Θ_{max} = 32.1°, reflections

collected/unique 20740/6207, R_{int} = 0.0556, R_1 = 0.0377, wR_2 = 0.1195, S = 1.123, largest diff. peak 0.500 e Å^{-3} and hole -0.756 e Å^{-3}.

Crystal structures of 1'- 4' determined from PXRD.

The crystal structures for narrow pore phases were solved from the PXRD patterns that were measured at room temperature on evacuated samples at the BESSY KMC-2 beamline of HZB. The data were collected in transmission geometry using 2 scans in the range of 5 to 50°. The patterns were indexed using the X-Cell program implemented in Material Studio 5.0 software.[20] The most intensive reflections in the 2Θ range between 2 and 20° were used for indexing. The $C222_1$ space group was chosen for **1', 2',** and **4'** considering group-subgroup relations and extinction rules. The starting models for the crystal structure refinement were derived from "as made" **1**, **2,** and **4** structures, which were converted into the corresponding space group. After adapting the unit cell parameters to those obtained during indexing, the structural models were optimized using geometry optimization tool with implementation of universal force field. Due to the low data/parameter ratio, the rigid-body Rietveld refinement with energy option was used to refine the structures.

Crystallographically independent Zn atoms, carboxylate groups, and phenyl rings were treated as rigid bodies.

In the case of compound **2'**, the minor impurity of open phase **2** is present after activation. Therefore, reflections at 7.0° and 11.6° 2Θ, which belongs to the open phase **2** (Fig. 3), were excluded from the Rietveld refinement.

Final Rietveld plots are given in Figure 1. CCDC-1422815, CCDC-1422817, CCDC-1422819, and CCDC-1422821 contain the supplementary crystallographic data for compounds **1'**, **2'**, **3'**, and **4'**, correspondingly. These data can be obtained free of charge from the Cambridge Crystallographic Data Centre *via* www.ccdc.cam.ac.uk/data_request/cif.

Refinement data for $Zn_3(bpydc)_2(HCOO)_2$ (1'): $C_{26}H_{14}N_4O_{12}Zn_3$, F_w = 770.58, Orthorhombic, $C222_1$ (*No.* 20), a = 27.821(1) Å, b = 10.184(1) Å, c = 21.626(1) Å, V = 6127.4(3) Å^3, Z = 8, 12 refined motion groups, 56 refined DOF, R_{wp} = 15.68 %, R_p = 12.20 %.

Refinement data for $Zn_3(bpydc)_2(CH_3COO)_2$ (2'): $C_{28}H_{18}N_4O_{12}Zn_3$, F_w = 798.63, Orthorhombic, $C222_1$ (*No.* 20), a = 27.715(1) Å, b = 10.575(1) Å, c = 21.691(1) Å, V = 6245.4(3) Å^3, Z = 8, 14 refined motion groups, 68 refined DOF, excluded regions 6.60 – 7.30, 11.50 – 11.77, R_{wp} = 7.60%, R_p = 5.83%.

Refinement data for $Zn_3(bpydc)_2(C_6H_5COO)_2$ (3'): $C_{38}H_{22}N_4O_{12}Zn_3$, F_w = 922.77, Tetragonal, $P4_32_12$ (*No.* 96), a = 15.019(1) Å, c = 21.905(2) Å, V = 4941.4(3) Å^3, Z = 4, 6 refined motion groups, 28 refined DOF, R_{wp} = 17.99 %, R_p = 12.10 %.

Refinement data for $Zn_3(bpydc)_2(C_6H_5CHCHCOO)_2$ (4'): $C_{42}H_{26}N_4O_{12}Zn_3$, F_w = 974.84, Orthorhombic, $C222_1$ (*No.* 20), a = 17.313 (1) Å, b = 24.594(1) Å, c = 22.139(2) Å, V = 9426.6(3) Å^3, Z = 8, 18 refined motion groups, 92 refined DOF, R_{wp} = 11.65%, R_p = 8.98 %.

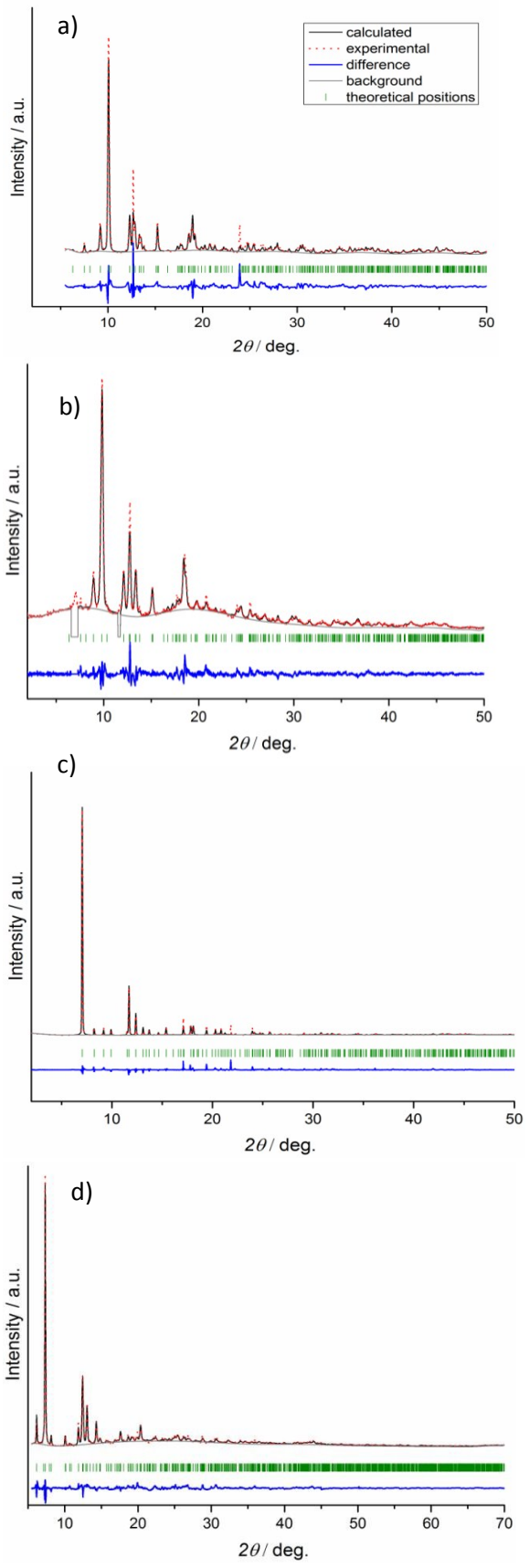

Figure 1. Rietveld plots for compounds **1'** (a), **2'** (b), **3'** (c), and **4'** (d).

***In situ* monitoring of nitrogen adsorption (77 K) by powder X-ray diffraction**

Concerted adsorption of N_2 at 77 K and X-ray powder diffraction experiments on compounds **3** and **4** were performed at KMC-2 beamline of HZB using specially designed instrumentation.[21] All adsorption experiments were performed at 195 K in the relative pressure range between 10^{-3} and 1 (p_0 = 101.3 kPa). All diffraction measurements were performed in 2Θ range from 2 to 50° using monochromatic synchrotron radiation (8048 eV; λ = 1.5406 Å). The diffraction images from 2D detector were integrated using Datasqueeze 2.2.9 software.[22] Hexagonal boron nitride was used as external standard.

Physical measurements

Thermogravimetric analyses were carried out under air using STA 409 PC from NETZSCH Company. Mass analysis was performed using Aëolos QMS 403 from NETZSCH Company. The heating rate was set to 5 K/min. FT-IR spectra were measured on VERTEX-70 spectrophotometer (Bruker) using DRIFT technique. Nitrogen adsorption measurements up to 100 kPa at 77K were performed on approximately 35 mg of sample using BELSORP-max apparatus. The nitrogen with the purity of 99.999% was used for the experiments. Powder X-ray diffraction patterns were measured on STADI P (Stoe) diffractometer at RT using monochromatic Cu–Kα_1 radiation (λ = 1.5406 Å) (step size: 0.05, exposure time: 23 sec/point) was used. All measurements were performed in transmission geometry. The samples were prepared in the Ar-filled Glovebox. Temperature dependent PXRD measurements were performed on Xpert diffractometer (PANALYTICAL) in reflection geometry using $\vartheta/2\vartheta$ scans and MRI (Material Research Instruments) sample stage. PXRD patterns were collected under dynamic vacuum every 25 °C in the temperature range between 25 and 450 °C . The heating rate was set to 3 K/min.

Results and Discussion

JLU-Liu4 developed by Liu and co-workers consists of the trinuclear Zn(II) units coordinated by four carboxylic groups, two 2,2'-bipyridine units, and two formate anions. The structure comprises of a 3D framework (**ant** topology) and displays channels 4.9 × 5.1 Å in dimensions.[13] 3D framework of JLU-Liu4 undergoes structural transformation upon removal of guest molecules from the pores to give a MOF with gate opening behavior. This is indicated by shifting and intensity changing of the peaks in the PXRD pattern. However, a structure of the desolvated compound was not reported yet.

To study the influence of monocarboxylic ligand nature on the structure formation of JLU-Liu4 (**1**), acetic (HAc), benzoic (HBz), or cinnamic (HCn) acids were used in the synthesis instead of originally reported formic acid.

In all cases crystalline products with the composition $Zn_3(bpydc)_2(Ac)_2$ (**2**), $Zn_3(bpydc)_2(Bz)_2$ (**3**), and $Zn_3(bpydc)_2(Cn)_2$ (**4**) could be obtained. Since all new materials could be obtained as crystals suitable for single crystal X-ray analysis, the crystal structures of all new materials were determined. All compounds crystallize in the same space group $P4_32_12$, and are isostructural, possessing similar frameworks with **ant** topology (Fig. 2a). As expected, the main difference in the structures is the monocarboxylic ligand included (Fig. 2b-2e). The volume of monocarboxylic anions (calculated as Connolly solvent excluded volume using ChemDraw software) and solvent accessible void volume change during activation are given in Scheme 1. According to the PLATON report, the solvent accessible void in the as made crystal structures changes from 59.4 % in **1** to 32.6 % in **4** (Table 1).

Table 1. Calculated textural properties of investigated compounds.

Compound	Solvent accessible void volume of unit cell / %	Calculated pore volume (V_p) / $cm^3\ g^{-1}$	Calculated geometrical surface area / $m^2\ g^{-1}$
1	59.4	0.70	2425
1'	17.6	0.09	76
2	55.7	0.63	2142
2'	15.8	0.09	66
3	40.5	0.36	1047
3'	36.7	0.30	690
4	32.6	0.30	747
4'	24.8	0.17	188

After removal of solvent molecules, crystallographic transformation takes place in all compounds, according to the changes in the PXRD patterns (Fig. 3). The patterns of all activated compounds (further referred as **1', 2', 3',** and **4',** respectively) were successfully indexed and the crystal structures were solved using molecular simulations combined with Rietveld refinement.

Activated phases **1'** and **2'** have very similar structures: both crystallize in the $C222_1$ space group with similar unit cell parameters (due to this similarity, only structure of **1'** is described in details below). The $C222_1$ space group is a sub-group of the $P4_32_12$ (the space group of the parent compounds **1** and **2**).

Due to the rigidity of the linker, the main contribution to the structural transformation comes from the cluster distortion. The reduction of the symmetry creates two independent SBUs (SBU 1 and SBU 2) in the **1'** showing differences in distortion with respect to the linearity of the Zn_3 array and coordination environment of the ligand molecules. In the SBU 1 the angle between three Zn atoms decreases from 178.65(1)° in **1** to 160.48(1)° in **1'.** The dihedral angle between oppositely located 2,2'-bipyridil rings changes from 80.31(5)° in **1** to 57.53(5)° in **1'** (Fig. 4a, 4b). A significant contribution to the structural contraction originates from bending of carboxylate hinges (dihedral angles between the plane of carboxylate group and O-Zn-Zn-O plane). These change from 5.75(3)° and 6.07(3)° in **1** to 19.42(3)° and 20.63(3)° in **1'**. This is also often the source of flexibility and structural transitions in other switchable MOFs .[23, 24] The Zn atoms in SBU 2 are arranged in nearly linear fashion with a Zn…Zn…Zn angle of 176.67(1)°. The formate anions, which are coordinated on the opposite sides of SBU in **1** (Fig. 4a, 4b) change the position in SBU 1 of **1'** and move to the same side of the cluster (Fig. 4b).

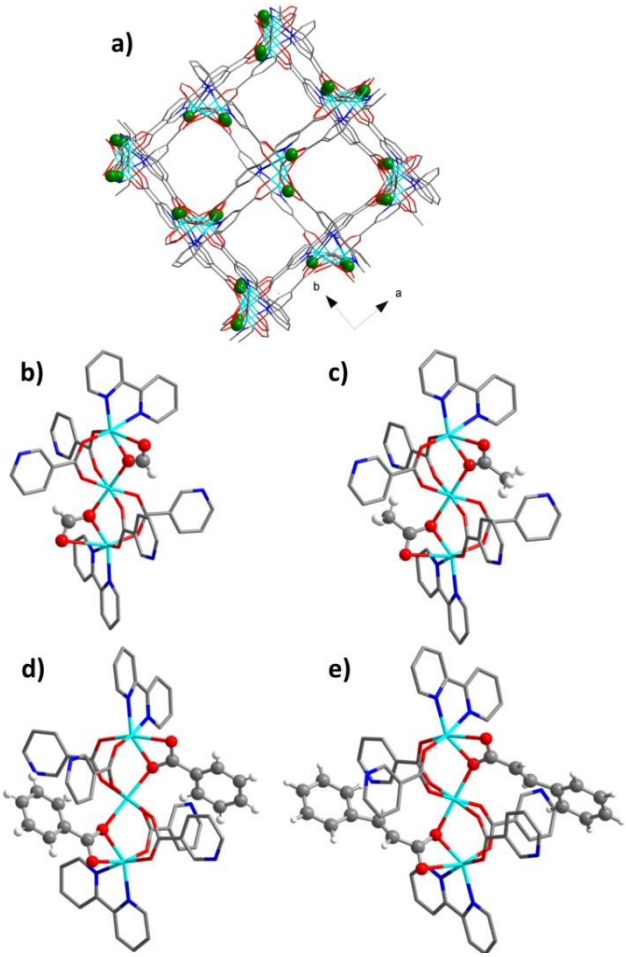

Figure 2. a) View on the structure of the JLU-LIU4 framework along *c* axis (green spheres represent monocarboxylate anions). b-e) Structure of SBUs in compounds **1** - **4**. Colour code: turquoise – Zn atoms, grey – carbon atoms, red – oxygen atoms, blue – nitrogen atoms.

On the framework level, the structural contraction in **1** occurs along [110] direction (Fig. 4c), corresponding to [010] direction in **1'** (Fig. 4d).

The textural properties of **1'** calculated using Poreblazer 3.0.2 software[25] show, that the compound has nearly no accessible pore volume (0.09 $cm^3 g^{-1}$) as well as very small pore limiting diameter of 2.11 Å. This completely supports the experimental results, since 1' shows no uptake of nitrogen up to reaching "gate opening pressure" of 0.47.

The crystal structure of compound **3'** was refined in the same space group as the structure of **3** (Fig. 1) with different lattice cell constants. Obviously, the compound **3** cannot undergo complete transformation because of bulky phenyl rings of the benzoate. It hinders the cluster transformation as it occurs in **1**. Namely, two coordinated benzoate anions, located on the opposite sides of the Zn cluster in **3** cannot regroup in the same way as in **1**, and are located on the same side of the SBU plane, because of the small aperture between the ligand molecules, coordinated to the cluster.

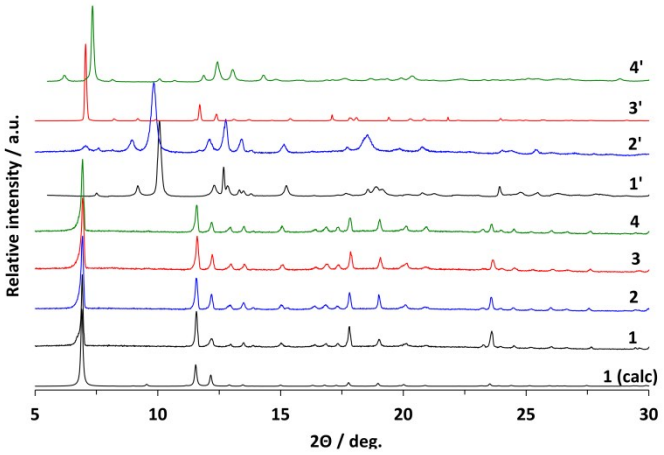

Figure 3. PXRD patterns for compounds **1 - 4** and **1' - 4'**.

The comparison of the calculated pore volumes for **3** and **3'** shows only minor changes from 0.36 $cm^3 g^{-1}$ to 0.30 $cm^3 g^{-1}$.

The thermal stability of the investigated materials was studied by temperature dependent PXRD and thermogravimetric (TG) analysis (Fig. S2 – S8 ESI). Investigation of the **1'** by thermo-XRD in argon atmosphere confirms retention of crystallinity up to 300 °C (see ESI, Fig. S1) confirming the TG data reported earlier.[13] According to TG analysis data, materials **2', 3',** and **4'** are stable up to 300 °C, 330 °C, and 320 °C, respectively (see ESI, Fig. S6 – S8). Therefore, the samples were activated at 150 °C in vacuum prior to the adsorption experiments.

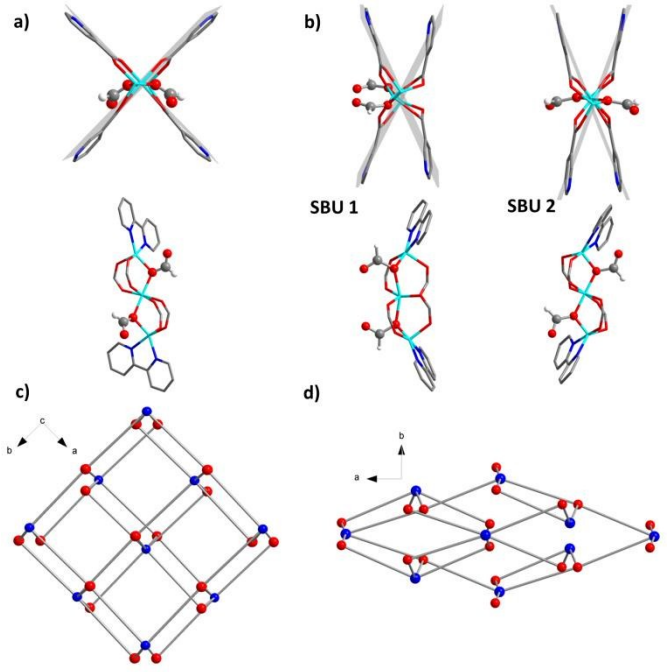

Figure 4. a) SBU 1 of **1**; b) SBU 1 and SBU 2 of **1'**; c) crystal structure of **1**; d) crystal structure of **1'**. (Colour code in (c) and (d): blue spheres – SBU units, red spheres – $bpydc^{2-}$ linkers).

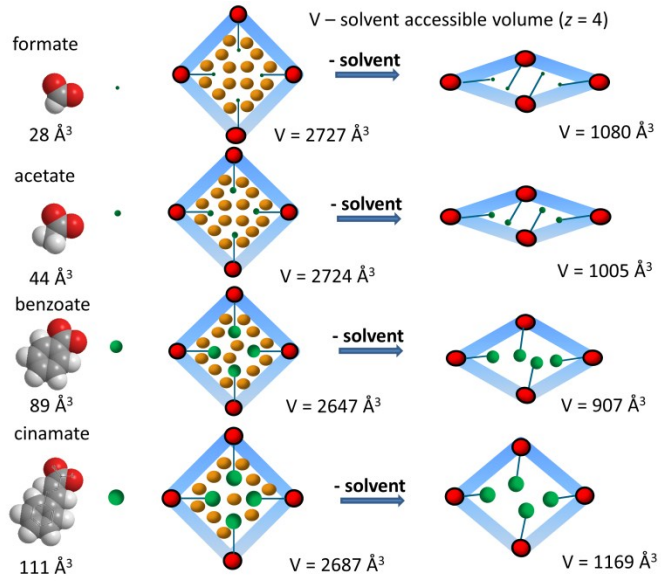

Scheme 1. Schematic representation of the monocarboxylic ligand influence on the activation of the LiU-4 series. The volume of monocarboxylic anions was calculated as Connolly solvent excluded volume using ChemDraw software. The volume of the cell represents the solvent accessible volume for $Z = 4$.

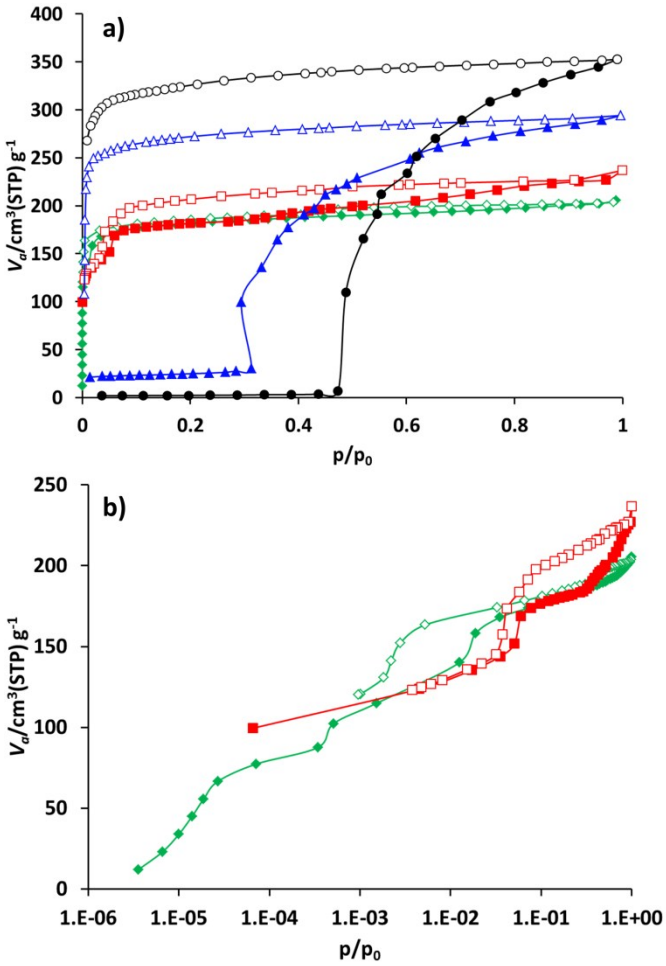

Figure 5. Nitrogen physisorption isotherms for compounds **1'**- **4'** at 77 K: a) linear representation of the isotherms; b) isotherms of compounds **3'** and **4'** in semilogarithmic scale. Black circles – **1'**, blue triangles – **2'**, red squares – **3'**, green diamonds – **4'**. Close symbols – adsorption, open symbols – desorption.

Compound **1'** shows classical gate pressure behaviour during physisorption of nitrogen at 77K, with almost no uptake up to $p/p_0 = 0.47$. The total pore volume calculated at $p/p_0 = 0.95$ amounts to 0.55 $cm^3 g^{-1}$ which is slightly lower than the theoretical value (Table 1). As expected, the nitrogen adsorption isotherm of **2'** shows a slightly different trend, reaching the plateau after adsorbing nearly 25 $cm^3 g^{-1}$ nitrogen at very low relative pressures. After reaching $p/p_0 = 0.3$ very steep increase in uptake takes place. The isotherm reaches a second plateau at $p/p_0 = 0.95$. The adsorbed amount in saturation is 295 $cm^3 g^{-1}$ that correspond to the pore volume of 0.456 $cm^3 g^{-1}$. Materials **3'** and **4'** show completely different behaviour during the adsorption of the nitrogen at 77 K (Fig. 5). Thus, compound **3'** adsorbs nearly 100 $cm^3 g^{-1}$ of nitrogen already at $p/p_0 = 10^{-4}$ confirming the incompleteness of crystal structure closing (narrow pore state) of **3'** discussed above. The second step in the isotherm, most likely connected to the structural transformation, occurs in the relative pressure range between 0.03 and 0.07. After that the course of the isotherm is characterized by the continuous increase of the uptake reaching 227 $cm^3 g^{-1}$ at $p/p_0 = 0.97$.

Implementation of the larger cinnamate anion into JLU-Liu4 has further influence on the adsorption properties of the solid. As in the case of **3'**, the hysteresis related to the guest induced structural changes is shifted to lower pressure range, and is located between $p/p_0 = 5{\cdot}10^{-3}$ and $p/p_0 = 5{\cdot}10^{-2}$. The isotherm reaches saturation at $p/p_0 = 0.95$ showing the nitrogen uptake of 203 $cm^3 g^{-1}$.

While the structural transformations during the adsorption of nitrogen on **1'** and **2'** is supposed to be one step "gate opening", the adsorption behaviour of **3'** and **4'** was studied by parallelized adsorption and PXRD experiments. PXRD patterns measured on evacuated material **3'** and at the first adsorption point (Fig. 6, PXRD No. 1) show the presence of narrow pore phase. Surprisingly, further five PXRD patterns, measured in the relative pressure range from $5{\cdot}10^{-4}$ up to 10^{-1} show a shift of the main (101) reflection from $2\theta = 7.19°$ to 7.44°, indicating the formation of an intermediate phase (ip) and contraction of the unit cell (Fig. 4, PXRD patterns No. 2 - 6). Unfortunately, the patterns could not be indexed unambiguously because of the presence of the reflections of more than one phase. Further increase of the gas pressure leads to the gradual shift of the (101) reflection back to lower angles, but the initial position is not completely reached (Fig. 4, PXRDs No 2 and 7). PXRD patterns, measured in the p/p_0 range of 0.1 to 1 are characterized by intensity increase of the reflection at $2\theta = 6.98°$, characteristic for the as made phase **3**. Although the PXRD patterns from 2 to 6 could not be indexed, the shape of the isotherm as well as reflection shift suggest that the transition is similar to breathing phenomena, observed in MIL-53(Cr) and MIL-53(Al) materials.[26] Desorption of nitrogen proceeds without phase transitions showing the presence of mixture of compounds **3'** and **3** up to low pressures. Only evacuation of the sample after the experiment at

room temperature leads to the structural transformation to the initial narrow pore state.

Nitrogen physisorption at 77 K combined with PXRD analysis on **4'** (Fig. 7) reveals completely different structural transformations induced by the cinnamate anion. The PXRD pattern of completely evacuated **4'** shows a reflection at 2ϑ = 7.50° matching the intermediate phase, obtained during the adsorption of nitrogen on **3'**. Indeed, the direct comparison of above mentioned PXRD patterns shows good match (Fig. S11, ESI). The indexing of the PXRD patterns obtained from evacuated **4'** gives several possible unit cells one of which is an orthorhombic *C*-centered one. Taking into account that **1'** crystallizes in the same crystal system, this unit cell was used for the Rietveld refinement. Pore volume calculated from the final structural model matches with value estimated from the adsorption isotherm of the compound.

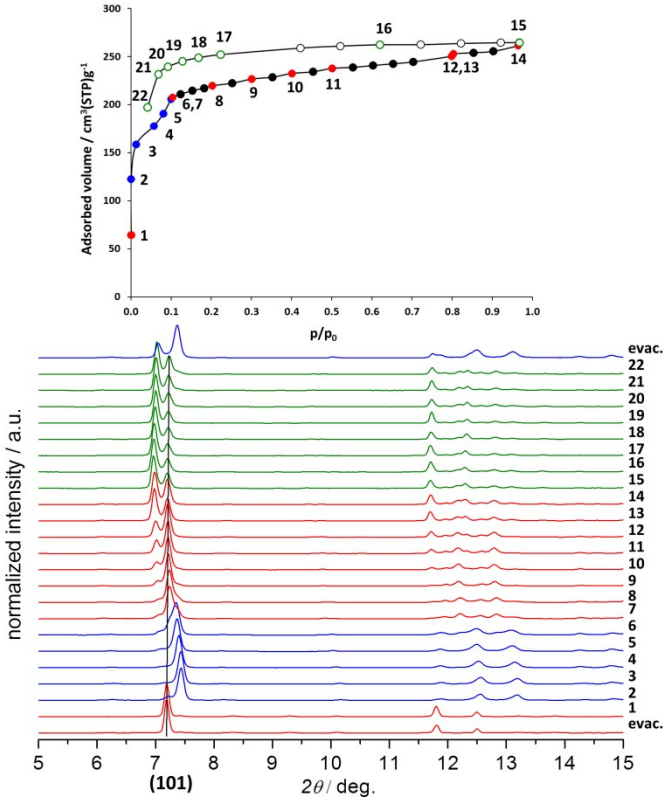

Figure 6. *In situ* adsorption of N_2 at 77K on **3'** by PXRD.

Although the adsorption isotherms of **3'** and **4'** are similar to some extent, *in situ* adsorption/PXRD experiments suggest a distinct pathway for the structural evolution in **4'**. In case of **4'**, the most intense reflection shifts towards lower 2θ angles with increasing pressure, probably indicating the stepwise opening of the crystal structure. The phase **4'** exists up to the relative pressure of 0.013. Further adsorption of nitrogen leads to phase transition, accompanied by the shift of most intense reflection from 7.50° to 7.29° 2θ. Unfortunately the pure intermediate phase could not be obtained and therefore PXRD patterns could not be indexed unambiguously. In the relative pressure range between 0.2 and 1 during the adsorption and desorption almost pure phase **4** is presented. Only at relative pressures lower than 10^{-2}, the reversible transformation from **4** to intermediate phase is observed.

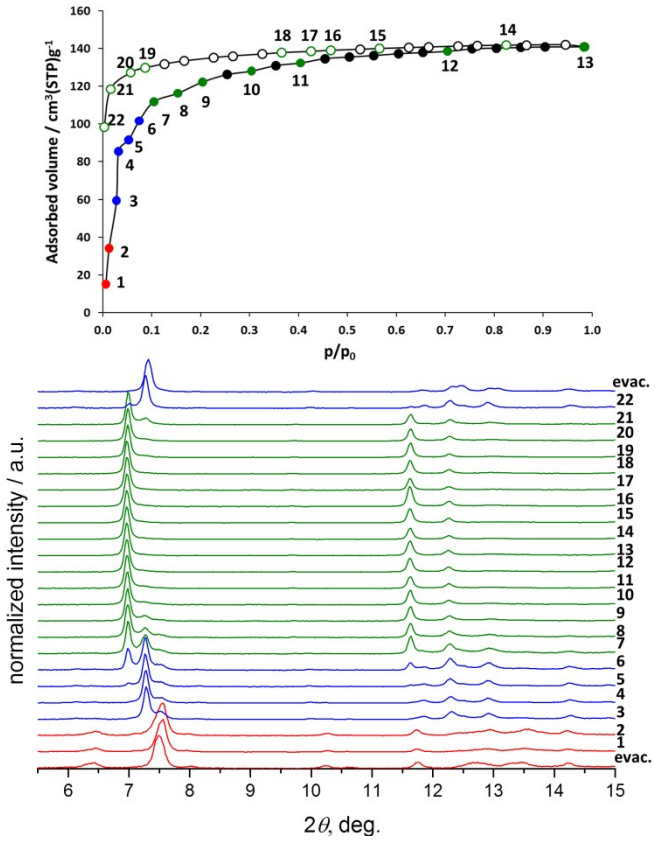

Figure 7. *In situ* adsorption of N_2 at 77K on **4'** by PXRD.

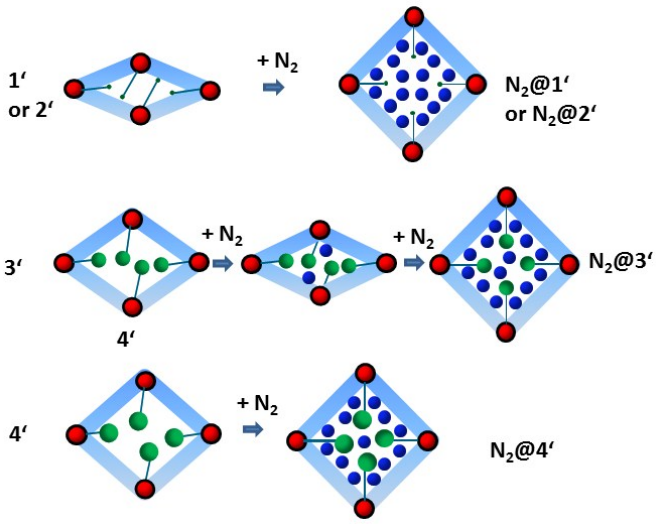

Scheme 2. Mechanisms of structural transformation during the adsorption of N_2 at 77 K for **1** - **4**.

Conclusions

In summary, the fine tuning of the gate pressure and switchability in JLU-Liu-4 was possible by modification of the SBU. Compounds containing coordinated formate, acetate, benzoate or cinnamate anions on cluster have the same frameworks with **ant** topology, but show variations in structural transformations during the adsorption of nitrogen at 77 K. While the utilisation of small carboxylic acids during the synthesis (compounds **1** and **2**) results in complete closing of the framework after solvent removal and therefore "gate opening" behaviour during the adsorption, bulkier carboxylates lead to incomplete closing of the frameworks after desolvation. Compounds containing benzoate (**3'**) and cinnamate (**4'**) anions show nearly the same adsorption behaviour but undergo completely different structural transformation during the adsorption. While the structural changes during adsorption on **3'** could be rather described as classical breathing,[27] the changes in **4'** lead to the step-wise increase of the unit cell volume. We believe, this approach can be further generalized and applied for other flexible MOFs with coordination vacancies on the metal cluster (typically Zn_3 and Co_3 clusters) in order to obtain materials with targeted adsorption properties.

Acknowledgements

N.K. thanks the "excellence initiative by the German federal and state government" (Institutional strategy, measure "support the best"). V.B. thanks the German Federal Ministry for education and research (Project BMBF No 05K13OD3). The HZB is gratefully acknowledged for the allocation of synchrotron radiation beamtime on KMC-2 and MX BL14.2 beamlines and for travel grants.

References

1. A. Schneemann, V. Bon, I. Schwedler, I. Senkovska, S. Kaskel and R. A. Fischer, *Chem. Soc. Rev.*, 2014, **43**, 6062-6096.
2. S. Horike, S. Shimomura and S. Kitagawa, *Nat Chem*, 2009, **1**, 695-704.
3. F.-X. Coudert, *Chem. Mater.*, 2015, **27**, 1905-1916.
4. P. Serra-Crespo, M. A. van der Veen, E. Gobechiya, K. Houthoofd, Y. Filinchuk, C. E. A. Kirschhock, J. A. Martens, B. F. Sels, D. E. De Vos, F. Kapteijn and J. Gascon, *J. Am. Chem. Soc.*, 2012, **134**, 8314-8317.
5. A. Douvali, A. C. Tsipis, S. V. Eliseeva, S. Petoud, G. S. Papaefstathiou, C. D. Malliakas, I. Papadas, G. S. Armatas, I. Margiolaki, M. G. Kanatzidis, T. Lazarides and M. J. Manos, *Angew. Chem. Int. Ed.*, 2015, **54**, 1651-1656.
6. H. Sato, W. Kosaka, R. Matsuda, A. Hori, Y. Hijikata, R. V. Belosludov, S. Sakaki, M. Takata and S. Kitagawa, *Science*, 2014, **343**, 167-170.
7. W. Kosaka, K. Yamagishi, A. Hori, H. Sato, R. Matsuda, S. Kitagawa, M. Takata and H. Miyasaka, *J. Am. Chem. Soc.*, 2013, **135**, 18469-18480.
8. Z. Chang, D.-H. Yang, J. Xu, T.-L. Hu and X.-H. Bu, *Adv. Mater.*, 2015, **27**, 5432-5441.
9. S. Henke, A. Schneemann, A. Wütscher and R. A. Fischer, *J. Am. Chem. Soc.*, 2012, **134**, 9464-9474.
10. P. Horcajada, F. Salles, S. Wuttke, T. Devic, D. Heurtaux, G. Maurin, A. Vimont, M. Daturi, O. David, E. Magnier, N. Stock, Y. Filinchuk, D. Popov, C. Riekel, G. Férey and C. Serre, *J. Am. Chem. Soc.*, 2011, **133**, 17839-17847.
11. O. Kozachuk, M. Meilikhov, K. Yusenko, A. Schneemann, B. Jee, A. V. Kuttatheyil, M. Bertmer, C. Sternemann, A. Pöppl and R. A. Fischer, *Eur. J. Inorg. Chem.*, 2013, **2013**, 4546-4557.
12. Y. Sakata, S. Furukawa, M. Kondo, K. Hirai, N. Horike, Y. Takashima, H. Uehara, N. Louvain, M. Meilikhov, T. Tsuruoka, S. Isoda, W. Kosaka, O. Sakata and S. Kitagawa, *Science*, 2013, **339**, 193-196.
13. J. Wang, J. Luo, J. Zhao, D.-S. Li, G. Li, Q. Huo and Y. Liu, *Cryst. Growth Des.*, 2014, **14**, 2375-2380.
14. P. Deria, Y. G. Chung, R. Q. Snurr, J. T. Hupp and O. K. Farha, *Chemical Science*, 2015, **6**, 5172-5176.
15. I. Gamba, I. Salvadó, G. Rama, M. Bertazzon, M. I. Sánchez, V. M. Sánchez-Pedregal, J. Martínez-Costas, R. F. Brissos, P. Gamez , J. L. Mascareñas, M. Vázquez López and M. E. Vázquez, *Chem. Eur. J.*, 2013, **19**, 13369-13375.
16. U. Mueller, N. Darowski, M. R. Fuchs, R. Forster, M. Hellmig, K. S. Paithankar, S. Puhringer, M. Steffien, G. Zocher and M. S. Weiss, *J. Synchrotron Rad.*, 2012, **19**, 442-449.
17. M. D. Winn, C. C. Ballard, K. D. Cowtan, E. J. Dodson, P. Emsley, P. R. Evans, R. M. Keegan, E. B. Krissinel, A. G. W. Leslie, A. McCoy, S. J. McNicholas, G. N. Murshudov, N. S. Pannu, E. A. Potterton, H. R. Powell, R. J. Read, A. Vagin and K. S. Wilson, *Acta Cryst. D*, 2011, **67**, 235-242.
18. G. Sheldrick, *Acta Cryst. A*, 2008, **64**, 112-122.
19. A. Spek, *Acta Cryst. D*, 2009, **65**, 148-155.
20. *Material Studio 5.0*, Accelrys Software Inc., San Diego, USA, 2009.
21. V. Bon, I. Senkovska, D. Wallacher, A. Heerwig, N. Klein, I. Zizak, R. Feyerherm, E. Dudzik and S. Kaskel, *Microporous Mesoporous Mater.*, 2014, **188**, 190-195.
22. P. A. Heiney, *Datasqueeze 2.2.9 Graphical Tool for X-ray Data Analysis*, 2012.
23. C. Serre, S. Bourrelly, A. Vimont, N. A. Ramsahye, G. Maurin, P. L. Llewellyn, M. Daturi, Y. Filinchuk, O. Leynaud, P. Barnes and G. Férey, *Adv. Mater.*, 2007, **19**, 2246-2251.
24. V. Bon, N. Klein, I. Senkovska, A. Heerwig, J. Getzschmann, D. Wallacher, I. Zizak, M. Brzhezinskaya, U. Mueller and S. Kaskel, *Phys. Chem. Chem. Phys.*, 2015, **17**, 17471-17479.
25. L. Sarkisov and A. Harrison, *Mol. Simul.*, 2011, **37**, 1248-1257.
26. C. Serre, F. Millange, C. Thouvenot, M. Noguès, G. Marsolier, D. Louër and G. Férey, *J. Am. Chem. Soc.*, 2002, **124**, 13519-13526.
27. G. Ferey and C. Serre, *Chem. Soc. Rev.*, 2009, **38**, 1380-1399.